Electronic Supplementary Material (ESI) for ChemComm.

Supporting information

On the formation of concentric 2D multicomponent assemblies at the solution-solid interface

Gangamallaiah Velpula[a], Takashi Takeda,[b,c] Jinne Adisoejoso[a], Koji Inukai[b] Kazukuni Tahara,[b,d] Kunal S. Mali,[a]* Yoshito Tobe[b]* and Steven De Feyter[a]*

[a]*Division of Molecular Imaging and Photonics, Department of Chemistry, KU Leuven-University of Leuven, Celestijnenlaan 200F, B-3001 Leuven, Belgium.*

[b]*Division of Frontier Materials Science, Graduate School of Engineering Science, Osaka University, Toyonaka, Osaka 560-8531, Japan.*

[c]*Present address: Institute of Multidisciplinary Research for Advanced Materials, Tohoku University, Sendai, Miyagi, 980-8577, Japan.*

[d]*Present address Department of Applied Chemistry, School of Science and Technology, Meiji University, 1-1-1 Higashimita, Tama-ku, Kawasaki, 214-8571, Japan.*

Corresponding authors: kunal.mali@kuleuven.be, tobe@chem.es.osaka-u.ac.jp, steven.defeyter@kuleuven.be

Contents:

Synthesis of DBA-(4)-OC10 and DBA-OC26

General. All reactions were performed under inert atmosphere (N_2 or Ar). All solvents were distilled or passed through activated alumina and copper catalyst in a Glass Contour solvent purification system prior use. All commercially available reagents were used as received.

^{1}H (400 MHz, 270 MHz) and ^{13}C (100 MHz, 67.5 MHz) NMR spectra were measured on Bruker UltraShield Plus 400 spectrometer, JEOL JNM AL-400 spectrometer or a JEOL JNM-GSX-270 spectrometer. For NMR measurements, chloroform-*d* was used as solvent, and the spectra were referenced to residual solvent proton signals in the ^{1}H NMR spectra (7.26 ppm) and to the solvent carbons in the ^{13}C NMR spectra (77.0 ppm), respectively. Other spectra were recorded by the use of the following instruments: IR spectra, JACSCO FT/IR-410; mass spectra, JEOL JMS-700 for EI or FAB ionization mode, AXIMA-CFR for LDI and JEOL JMS-S3000 for MALDI ionization mode.

Synthesis of DBA-(4)-OC10. Synthesis of **DBA-(4)-OC10** was accomplished through a synthetic route shown in Scheme S1.

Scheme S1. Synthesis of **DBA-(4)-OC10**.

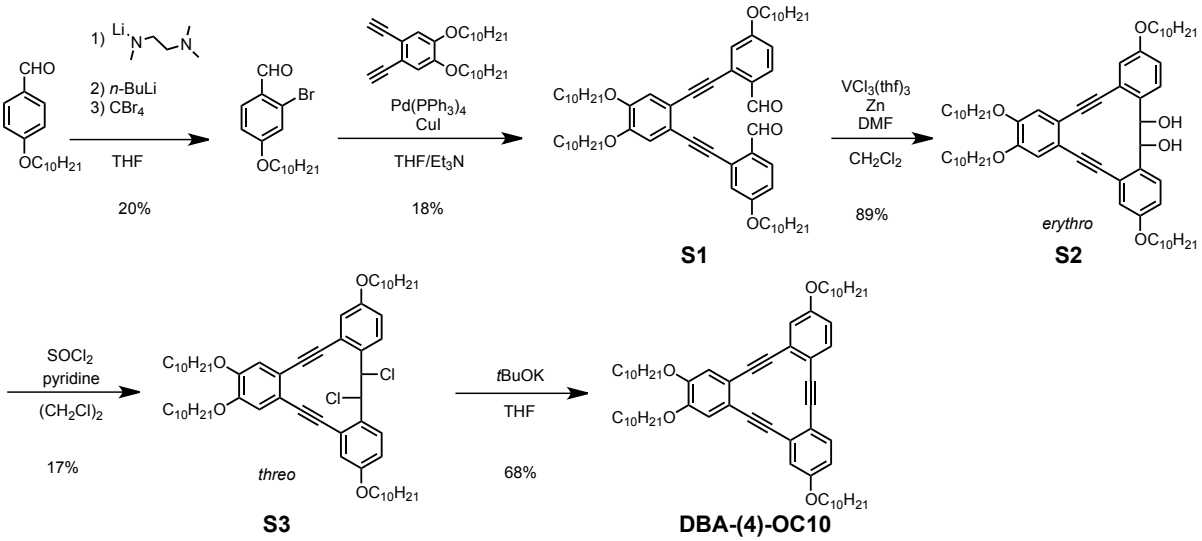

Synthesis of 2-Bromo-4-decyloxybenzaldehyde. Preparation of this compound was performed by following the literature.[1] To a solution of *N*,*N*,*N'*-triethylethylenediamine (4.90 mL, 33.1 mmol) in THF

(50 mL) was added *n*-butyllithium (1.67 M in hexane, 18.9 mL, 31.6 mmol) at –20 °C. The mixture was stirred at –20 °C - –25 °C for 35 min. Then, 4-decyloxybenzaldehyde (3.85 mL, 15.0 mmol) was added dropwise. After stirring at same temperature for 35 min, *n*-butyl lithium (1.67 M in hexane, 22.5 mL, 37.6 mmol) was added dropwise. The mixture was further stirred at –20 °C - –25 °C for 2 h. After the mixture was cooled to –78 °C, carbon tetrabromide (24.9 g, 75.1 mmol) was added. The mixture was allowed to warm gradually to room temperature and stirred for 15 h. After addition of 2 M HCl aq., the mixture was extracted with ether. Combined organic layer was washed with 2 M HCl aq., sat. $Na_2S_2O_3$ aq., and brine and dried over $MgSO_4$. After removal of the solvents under reduced pressure, the crude mixture was subject to the silica gel column chromatography (eluent hexane/$CHCl_3$ = 1/1) to give 2-bromo-4-decyloxybenzaldehyde (1.01 g, 20%) as a yellow oil. ^{1}H NMR (400 MHz, $CDCl_3$) δ 10.21 (d, *J* = 0.8 Hz, 1H), 7.87 (d, *J* = 8.5 Hz, 1H), 7.12 (d, *J* = 2.3 Hz, 1H), 7.08 (ddd, *J* = 8.8, 2.3, 0.7 Hz, 1H) 4.02 (t, *J* = 6.5 Hz, 2H) 1.84–1.75 (m, 2H), 1.50–1.40 (m, 2H), 1.40–1.21 (m, 12H), 0.88 (m, 3H); ^{13}C NMR (100 MHz, $CDCl_3$) δ 190.5, 164.2, 131.3, 128.7 126.8, 119.0, 114.4, 68.8, 31.8, 29.5, 29.25, 29.23, 28.9, 25.8, 22.6, 14.0; IR (neat) 2925, 2854, 1688, 1592, 1488, 1468, 1390, 1299, 1238, 1027, 863, 842, 651, 628 cm^{-1}; HR-MS (EI) calcd. for $C_{17}H_{25}O_2{}^{79}Br$ 340.1038, found 340.1064.

Synthesis of Bis(ethynylbenzaldehyde) S1. To a solution of 1,2-bis(decyloxy)-4,5-diethynylbenzene[2] (411 mg, 936 μmol) and 2-bromo-4-decyloxybenzaldehyde (690 mg, 2.02 mmol) in a mixture of Et_3N (15 mL) and THF (30 mL) were added $Pd(PPh_3)_4$ (108 mg, 93.6 μmol) and CuI (35.6 mg, 187 μmol). The mixture was stirred at 60 °C for 6.5 h. To the mixture, Et_2O and sat. NH_4Cl aq. were added and aqueous layer was extracted with ether. Combined organic layer was washed with sat. NH_4Cl aq. and brine, then dried over $MgSO_4$. After evaporation of the solvents under vacuum, the crude mixture was subject to the silica gel column chromatography (hexane/$CHCl_3$; from 2/1 to 1/1) to give the dialdehyde **S1** as an orange solid (165 mg, 18%). mp 68–69 °C; ^{1}H NMR (400 MHz, $CDCl_3$) δ 10.56 (d, *J* = 0.8 Hz, 2H), 7.87 (d, *J* = 8.5 Hz, 2H), 7.06 (d, *J* = 2.4 Hz, 2H), 7.05 (s, 2H), 6.94 (ddd, *J* = 8.8, 2.4, 0.8 Hz, 2H) 4.05 (t, *J* = 6.6 Hz, 4H), 3.97 (t, *J* = 6.5 Hz, 4H), 1.91–1.82 (m, 4H), 1.82–1.73 (m, 4H), 1.55–1.17 (m, 56H), 0.92–0.80 (m, 12H); ^{13}C NMR (100 MHz, $CDCl_3$) δ 190.3, 163.5, 149.9, 129.4, 129.3 128.9, 117.9,

117.0, 116.4, 116.1, 94.9, 87.9, 69.4, 68.5, 31.91, 31.89, 29.60, 29. 56, 29.4, 29.34, 29.31, 29.1, 29.0, 26.0, 25.9, 22.7, 14.1; IR (KBr) 2955, 2920, 2872, 2851, 2210, 1682, 1598, 1516, 1467, 1366, 1226, 1088, 861, 846, 819 cm^{-1}; HR-MS (FAB) calcd. for $C_{64}H_{95}O_6$ (M+H) 959.7129, found 959.7134.

Synthesis of Diol S2. A suspension of VCl_3 (481 mg, 3.06 mmol) in dry THF (10 mL) was stirred at 75 °C under nitrogen for 16 h. After cooling the mixture to –78 °C, the supernatant liquid was removed via a syringe. The resulting pink solid was washed with pentane thrice. After removal of remaining solvent under reduced pressure, Zn (220 mg, 3.36 mg atom) and dry CH_2Cl_2 (20 mL) were added. The mixture was stirred for 15 min at room temperature. Then dry DMF (300 μL) was added and the mixture was stirred for additional 40 min. To the resulting green suspension, a solution of the dialdehyde **S1** (85.1 mg, 88.7 μmol) in dry CH_2Cl_2 (5 mL) was added dropwise. The mixture was stirred for 30 min at room temperature. After dilution with $CHCl_3$ and 1 M HCl aq., aqueous layer was extracted with $CHCl_3$. Combined organic layer was washed with 1 M HCl aq. and brine, and dried over $MgSO_4$. After removal of the solvents under reduced pressure, the resulting mixture was purified by the silica gel column chromatography (hexane/AcOEt = 10/1) to give an *erythro*-diol (75.5 mg, 89%) as an orange solid. mp 112–113 °C; ^{1}H NMR (400 MHz, $CDCl_3$) δ 7.72 (d, *J* = 8.5 Hz, 1H) 7.32 (d, *J* = 8.5 Hz, 1H), 7.24 (d, *J* = 2.8 Hz, 1H), 7.13 (d, *J* = 2.5 Hz, 1H), 7.08 (s, 1H), 7.05 (s, 1H), 7.04 (dd, *J* = 8.5, 2.5 Hz, 1H), 6.90 (dd, *J* = 8.5, 2.5 Hz, 1H), 5.67 (dd, *J* = 9.5, 2.8 Hz, 1H), 4.39 (dd, *J* = 11.3, 9.5 Hz, 1H), 4.06-3.98(m, 8H), 3.41(d, *J* = 11.3 Hz, 1H) 1.88–1.79 (m, 8H), 1.77 (d, *J* = 2.8 Hz, 1H), 1.52–1.20 (m, 56H) 0.93–0.85 (m, 12H); ^{13}C NMR (100 MHz, $CDCl_3$) δ 158.2, 157.8, 148.9, 148.7, 137.9, 136.1, 132.2, 126.3, 122.8, 120.0, 119.0, 118.04, 118.01, 116.0, 114.9, 114.7, 114.0, 94.7, 92.7, 90.9, 89.7, 81.7, 71.0, 68.9, 68.8, 67.88, 67.86, 31.59, 31.57, 29.3, 29.27, 29.26, 29.1, 29.03, 28.99, 28.96, 28.51, 28.49, 25.8, 25.7, 25.5, 22.3, 13.8; IR (KBr) 3500, 3409, 3309, 2955, 2923, 2853, 1597, 1567, 1509, 1469, 1355, 1307, 1247, 1224, 1069, 1032, 859, 831, 722 cm^{-1}; HRMS (FAB) calcd. for $C_{64}H_{96}O_6$ 960.7207, found 960.7212.

Synthesis of Dichloride S3. To a solution of the *erythro*-diol **S2** (75.5 mg, 78.5 μmol) in 1,2-dichloroethane (5 mL) was added pyridine (35 μL) and thionyl chloride (25 μL). The mixture was stirred at room temperature for 2 h. After addition of 1 M HCl aq., the mixture was extracted with $CHCl_3$.

Combined organic layer was washed with 1 M HCl aq., and brine and dried over $MgSO_4$. After removal of the solvents under reduced pressure, the product was separated by the silica gel column chromatography (hexane/$CHCl_3$ = 5/1) to give a *threo*-dichloride (13.0 mg, 17%) as a white solid. mp 153–155 °C; ^{1}H NMR (400 MHz, $CDCl_3$) δ 7.89 (d, *J* = 8.8 Hz, 2H), 7.11 (d, *J* = 2.8 Hz, 2H), 7.09 (s, 2H), 6.99 (dd, *J* = 9.0, 2.8 Hz, 2H), 5.70 (s, 2H), 4.06–3.98 (m, 8H), 1.91–1.76 (m 8H), 1.53–1.19 (m, 56H), 0.93–0.83 (m, 12H); ^{13}C NMR (100 MHz, $CDCl_3$) δ 158.5, 149.6, 132.5, 132.2, 121.3, 118.8, 116.1, 115.3, 114.8, 94.0, 89.9, 69.3, 68.2, 64.1, 31.92, 31.90, 29.62, 29.58, 29.56, 29.40, 29. 36, 29.32, 29.2, 29.12, 29.06, 26.0, 22.7, 14.1; IR (KBr) 2954, 2923, 2854, 2207, 1598, 1569, 1511, 1499, 1467, 1397, 1362, 1322, 1289, 1269, 1247, 1223, 1065, 1022, 876, 849, 826, 721, 667, 620, 599, 570 cm^{-1} ;HR-MS (FAB) calcd. for $C_{64}H_{94}O_4{}^{35}Cl_2$, 996.6529, found 996.6582.

Synthesis of DBA-(4)-OC10. To a suspension of potassium *tert*-butoxide (102 mg, 909 μmol) in THF (1 mL) was added dropwise a solution of the *threo*-dichloride **S3** (13.0 mg, 130 μmol) in dry THF (4 mL). The mixture was stirred for 16 h at room temperature under nitrogen. After quenching with 1 M HCl aq., the mixture was extracted with $CHCl_3$. Combined organic layer was washed with brine and dried over $MgSO_4$. The crude mixture was subject to silica gel column chromatography (hexane/$CHCl_3$ = 2/1) to give the **DBA-(4)-OC10** (8.3 mg, 68%) as a yellow solid. mp 78–79 °C; ^{1}H NMR (400 MHz, $CDCl_3$) δ 7.16 (d, *J* = 8.5 Hz, 2 H), 6.80 (d, *J* = 2.5 Hz, 2H), 6.79 (s, 2H), 6.68 (dd, *J* = 8.5, 2.5 Hz, 2H), 3.98 (t, *J* = 6.6 Hz, 4H), 3.93 (t, *J* = 6.4 Hz, 4H), 1.86–1.72 (m, 8H), 1.52–1.20 (m, 56H), 0.97–0.82 (m, 12 H); ^{13}C NMR (100 MHz, $CDCl_3$) δ 158.8, 149.5, 132.8, 127.8, 119.7, 119.2, 116.8, 116.1, 115.5, 92.9, 91.7, 91.5, 69.1, 68.2, 31.91, 31.89, 29.60, 29.56, 29.54, 29.37, 29.34, 29.31, 29.15, 29.12, 26.0, 22.7, 14.1; IR (KBr) 2941, 2923, 2869, 2850, 2213, 1598, 1554, 1505, 1465, 1395, 1356, 1327, 1300, 1268, 1245, 1222, 1068, 1019, 861, 846, 824 cm^{-1}; HR-MS (FAB) calcd. for $C_{64}H_{92}O_4$ 924.6996, found 924.7018.

Synthesis of DBA-OC26. *tert*-Butyldimethylsilyl protected hexahydroxyDBA (10.8 mg, 10.0 μmol)[3] and CsF (15.2 mg, 100 μmol) were suspended in DMF (1.0 mL) in a Schlenk tube. After addition of 1-$C_{26}H_{53}Br$ (44.6 mg, 100 μmol), the mixture was stirred at 80 °C for 24 h. The solvent was removed under vacuum. The resulting mixture was dissolved in hot $CHCl_3$, the solution was subjected to the

silica gel column chromatography ($CHCl_3$), and then recrystallization from $CHCl_3$/EtOH afforded **DBA-OC26** (22.0 mg, 85%) as a yellow solid. mp 80.1–81.3 °C; ^{1}H NMR (270 MHz, $CDCl_3$, 30 °C) δ 6.72 (s, 6H), 3.95 (t, *J* = 6.6 Hz, 12H), 1.80 (quint, *J* = 6.6 Hz, 6H), 1.59–1.16 (m, 276H), 0.89 (t, *J* = 6.3 Hz 18H); ^{13}C NMR (67.5 MHz, $CDCl_3$, 30 °C) δ 149.1, 119.8, 115.9, 91.9, 69.2, 32.0, 29.80, 29.75, 29.5, 29.4, 29.3, 26.1, 22.8, 14.2; IR (KBr) 2919, 2850, 1509, 1469, 1349, 1227 cm^{-1}; HR-MS (MALDI) calcd. for C180H324O6 2582.5043, found 2582.5065.

References

1. J. F. Bower, P. Szeto and T. Galagher, *Org. Biomol. Chem.* **2007**, *5*, 143–150.

2. Q. Zhou, P. J. Carroll and T. M. Swager, *J. Org. Chem.* **1994**, *59*, 1294–1301

3. K. Tahara, S. Lei, D. Mössinger, H. Kozuma, K. Inukai, M. van der Auweraer, F. C. De Schryver, S. Höger, Y. Tobe and S. De Feyter, *Chem. Commun.* **2008**, 3897–3899.

Experimental details: STM

Commercially available coronene (Aldrich 97%) isophthalic acid (Acros Co. 99%), octanoic acid (Sigma Lifescience. ≥ 99%) were used as received. Stock solutions of coronene (2.0×10^{-3} M), isophthalic acid (6.0×10^{-3} M), dehydrobenzo[12]annulene derivatives **DBA-OC26** (3.9×10^{-4} M) and **DBA-(4)-OC10** (1.0×10^{-3} M) were prepared by dissolving appropriate amount of solid in octanoic acid. Octanoic acid was chosen as the solvent due to the fact of isophthalic acid is readily soluble in it. The stock solutions were diluted further to make concentration series. All STM experiments were performed at room temperature (21–23^{0}C) using a PicoSPM (Molecular imaging, now Keysight) machine operating in constant-current mode with the tip immersed in the supernatant liquid. STM tips were prepared by mechanically cutting a Pt/Ir wire (80%/20%, diameter 0.2 mm). Prior to imaging, a drop of warm 4-component solution was placed onto a freshly cleaved surface of highly oriented pyrolytic graphite (HOPG, grade ZYB, Advanced Ceramics Inc., Cleveland, USA). Deposition of solution at room temperature also provide comparable results. The experiments were repeated in 2-3 sessions using different tips to check for reproducibility and to avoid experimental artefacts, if any. The multicomponent networks are typically formed over a range of composition. For analysis purposes, recording of a monolayer image was followed by imaging the graphite substrate underneath it under the same experimental conditions, except for increasing the current and lowering the bias. The images were corrected for drift via Scanning Probe Image Processor (SPIP) software (Image Metrology ApS), using the recorded graphite images for calibration purposes, allowing a more accurate unit cell determination. The unit cell parameters were determined by examining at least 4 images and only the average values are reported. The images are Gaussian filtered. The imaging parameters are indicated in the figure caption: sample bias (V_{bias}) and tunneling current (I_{set}). The molecular models were built using Hyperchem^{TM} 7.0 program. For the statistical analysis of the handedness of inner (DBA-4-OC10) and outer (DBA-OC26) shells, a total of 125 ordered four-component hexagons were examined. Distorted hexagons are observed less frequently however a total of 17 distorted hexagons revealed that both the inner as well as outer DBA shells show distortion in alkyl chain interdigitation pattern.

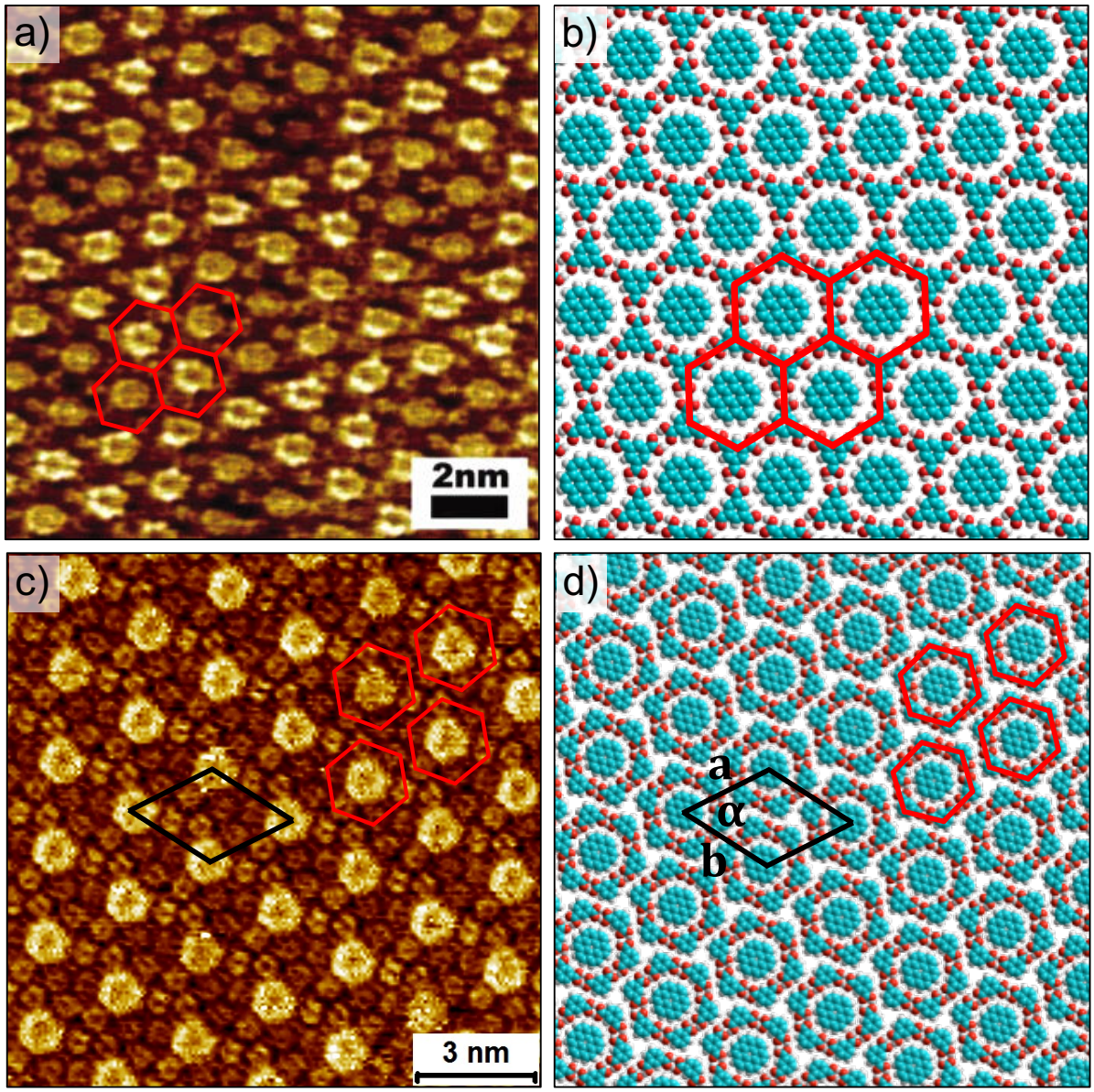

Fig. S1 Design strategy: Extended honeycomb versus close-packed hexagonal networks (**COR-TMA** *versus* **COR-ISA**) (a) STM image of the **COR-TMA** host-guest network. Reproduced from *Langmuir,* **2004,** *20,* 9403-9407. (b) Molecular model for the **COR-TMA** system. (c) STM image of the **COR-ISA** host-guest network (d) Molecular model for the **COR-ISA** system. Note that **TMA** forms an extended honeycomb network, where the hexagons are connected to each other (red) through hydrogen bonds whereas in the **COR-ISA** system, the individual hexagons are close-packed and interact with each other only *via* van der Waals interactions.

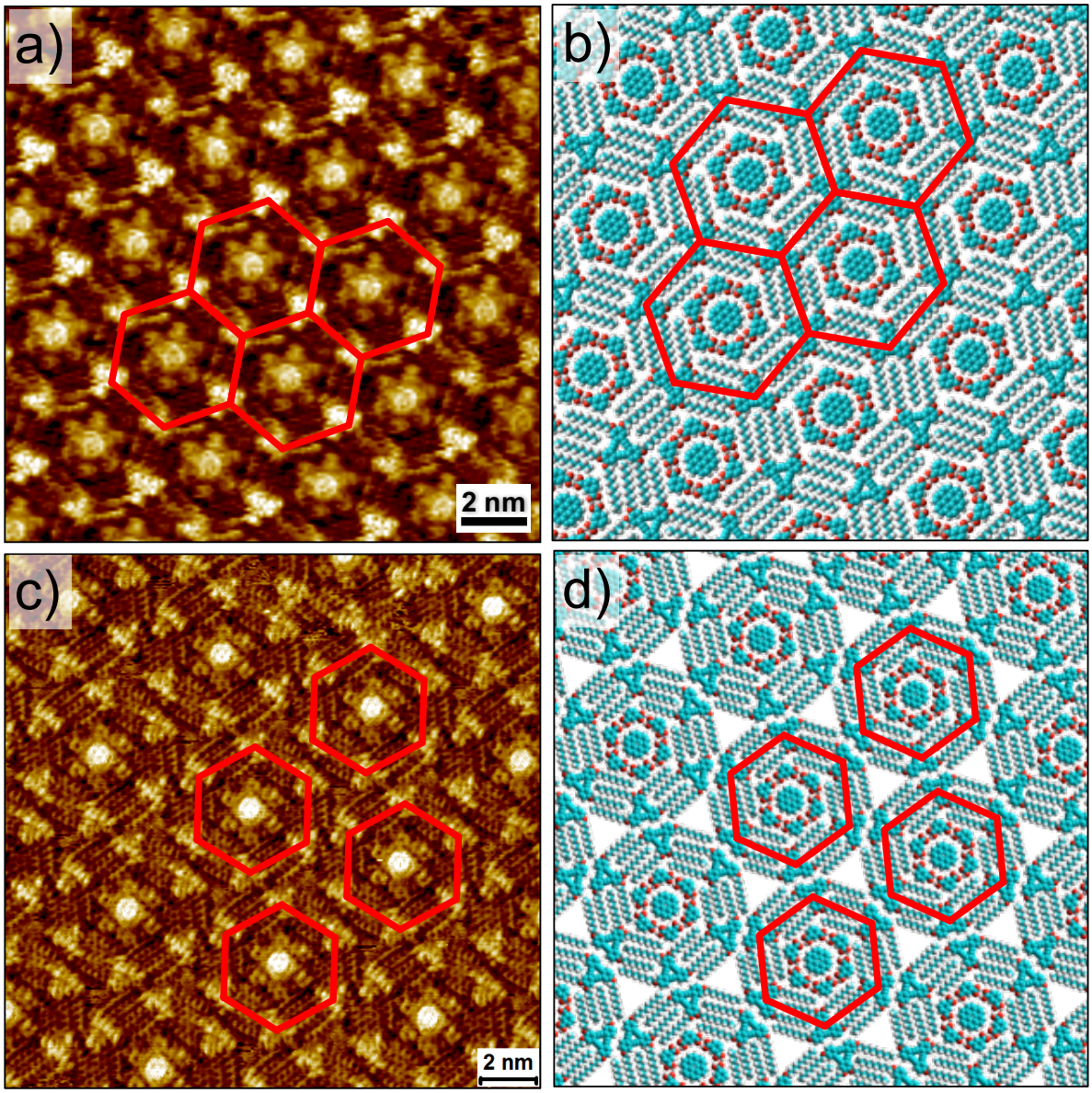

Fig. S2 Design strategy: Extended honeycomb versus close-packed hexagonal networks (**DBA-OC10-ISA-COR v*ersus* DBA-(4)-OC10-ISA-COR**) (a) STM image of the **DBA-OC10-ISA-COR** host-guest network (b) Molecular model for the **DBA-OC10-ISA-COR** system. (c) STM image of the **DBA-(4)-OC10-ISA-COR**) host-guest network (d) Molecular model for the **DBA-(4)-OC10-ISA-COR** system. Note that **DBA-OC10-ISA-COR** forms an extended honeycomb network, where the hexagons are connected to each other (red) through interdigitated alkyl chains whereas in the **DBA-(4)-OC10-ISA-COR** system, the individual hexagons are only close-packed. This difference allows **DBA-(4)-OC10-ISA-COR** to act as a discrete guest for the **DBA-OC26** cavity.

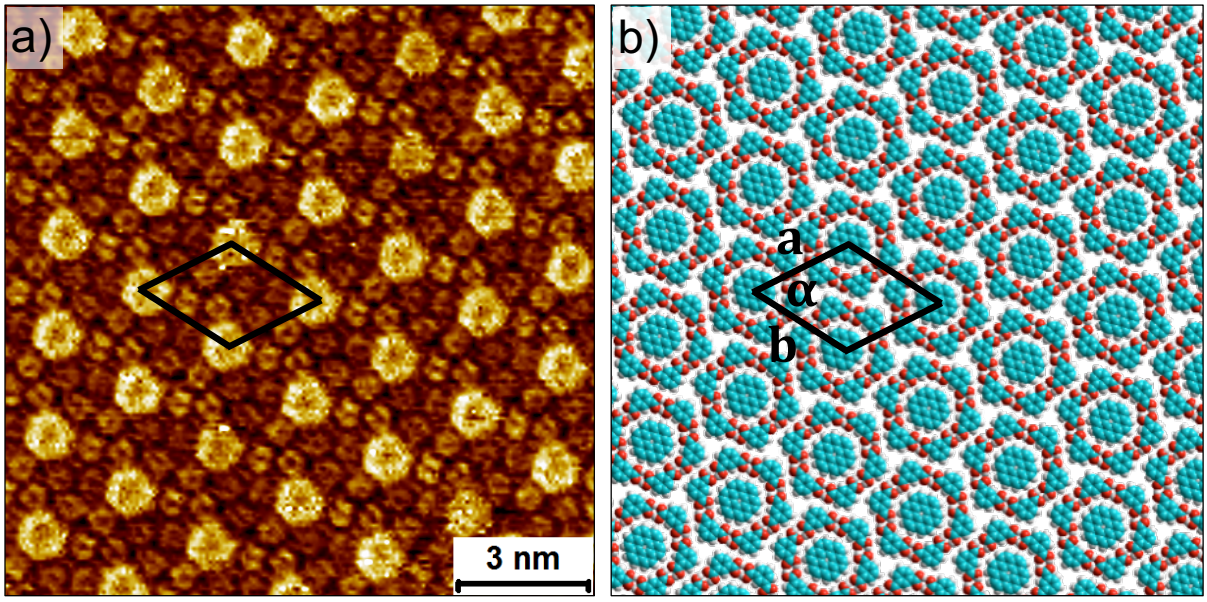

Fig. S3 (a) STM image showing the two-component **COR-ISA** self-assembled network formed at the octanoic acid/HOPG interface. Each **COR** molecule is surrounded by six molecules of **ISA**. (b) Molecular model for the **COR-ISA** network. Imaging parameters: V_{bias} = 400 mv, I_{set} = 0.27 nA. The unit cell contains 7 molecules. 1 **COR** and 6 **ISA**.

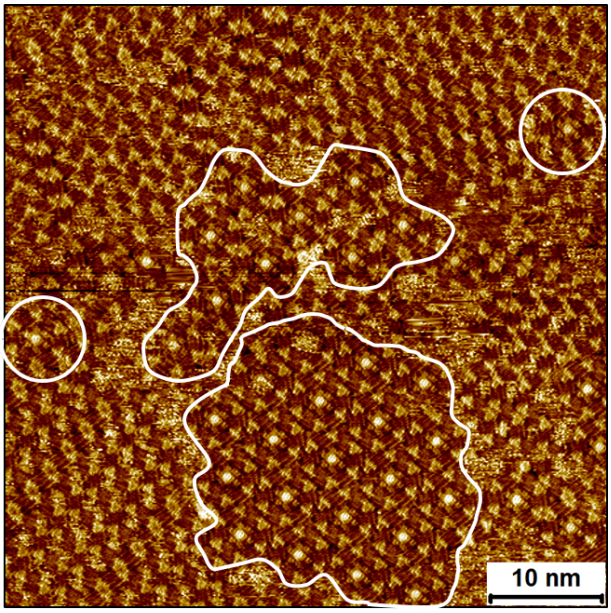

Fig. S4 Large-scale STM image of the three-component system formed at the octanoic acid/HOPG interface. **DBA-(4)-OC10** (5.5×10^{-6} M), **COR** (1.1×10^{-4} M) and **ISA** (3.5×10^{-4} M). Apart from the desired three-component network comprising **DBA-(4)-OC10-ISA-COR** clusters, phase separated domains of **DBA-(4)-OC10** are also formed. White lines and circles separate the three-component domains from the densely packed phase of **DBA-(4)-OC10**. Imaging parameters: V_{bias} = 450 mV, I_{set} = 0.180 nA.

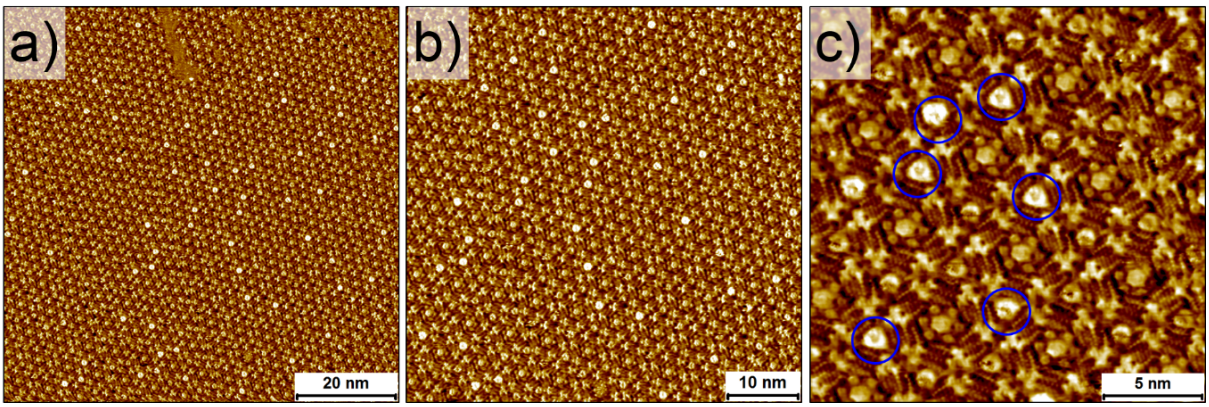

Fig. S5 Additional STM images of the three-component Kagomé network obtained at the octanoic acid/HOPG interface. Note that the domain size is significantly larger than the three component network described before (Fig. S2 and Fig. 2 in the main text). Solution composition: **DBA-(4)-OC10** (3.2×10^{-6} M), **ISA** (2.7×10^{-4} M) and **COR** (2.3×10^{-5} M). We note that this composition is slightly different than the one in Figure 3. However, the network is obtained over a range of composition. Imaging parameters: V_{bias} = -1.0 V, I_{set} = 0.07 nA. Some **COR** molecules that occupy the interstitial triangular sites appear brighter than others (blue circles) indicating a possibility of formation higher order stacks.

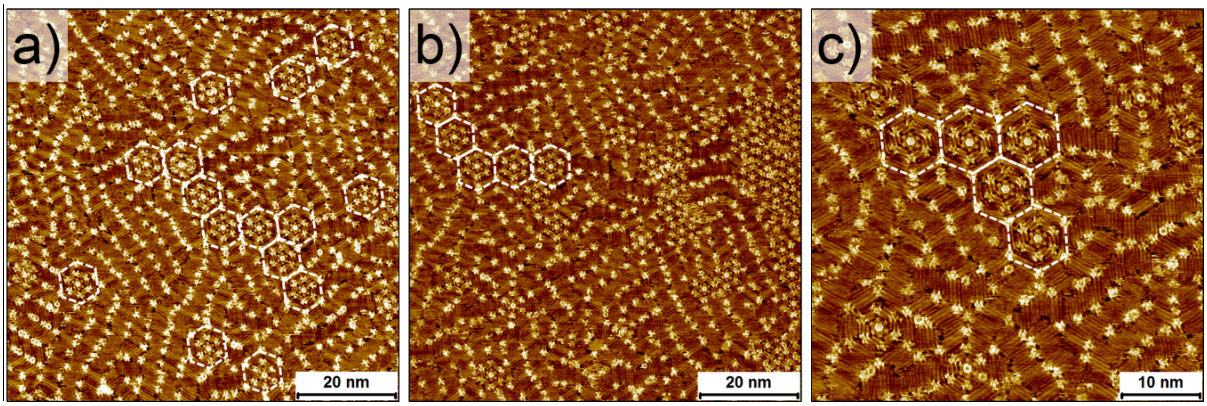

Fig. S6 (a-c) Additional large-scale STM images of the four-component system obtained at the octanoic acid/HOPG interface. Solution composition: **DBA-OC26** (2.8×10^{-6} M), **DBA-(4)-OC10** (3.2×10^{-6} M), **COR** (2.3×10^{-5} M) and **ISA** (2.7×10^{-4} M). Imaging parameters: V_{bias} = -1.0 V, I_{set} = 0.07 nA. It is clearly evident that the four-component concentric clusters (white dotted lines) co-exist with the densely packed network of **DBA-OC26**.

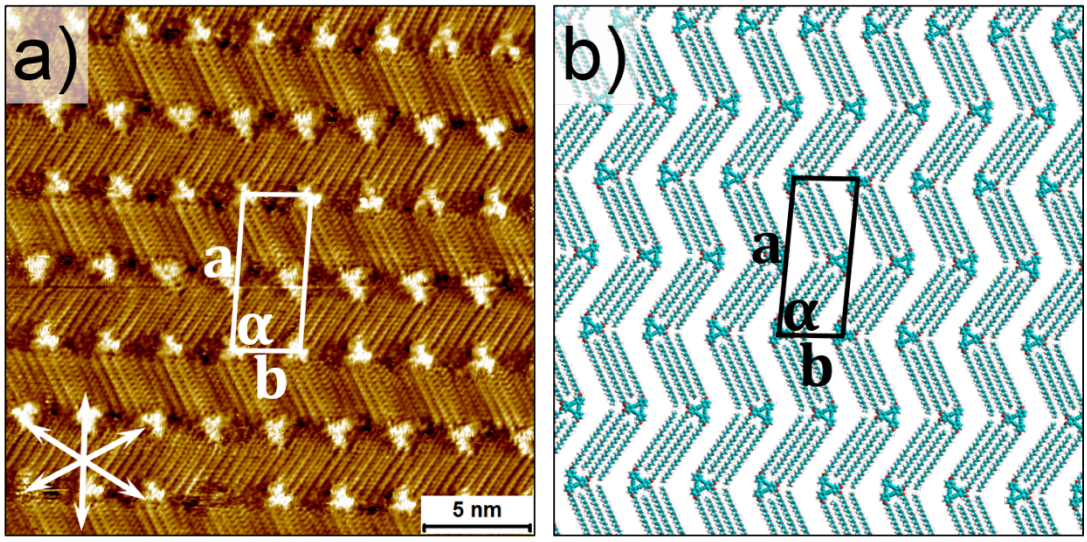

Figure S7: (a) High-resolution STM image of the densely packed structure of **DBA-OC26** formed at the octanoic acid/HOPG interface. The graphite symmetry axes are shown in the lower left corner. The unit cell is overlaid on the STM image and the cell parameters are: a = 7.3±0.1 nm, b= 3.0±0.1 nm and α = 86±1.0°. Imaging parameters: V_{bias} = 400 mV, I_{set} = 0.27 nA. (b). Molecular model showing the arrangement of **DBA-OC26** molecules in the self-assembled monolayer. The molecules are shown only with four alkyl chains for the sake of clarity, although five alkoxy chains per molecule are adsorbed. The unit cell contains 2 molecules.

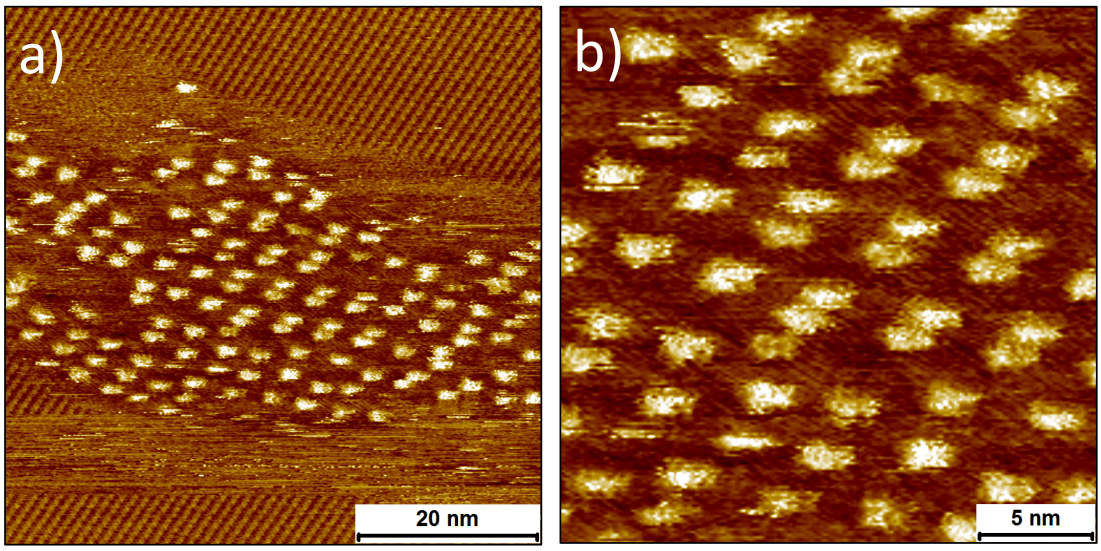

Figure S8: Large-scale (a) and small-scale (b) STM images of the **DBA-OC26** network obtained at 7.7 × 10^{-7} M concentration at octanoic acid/HOPG interface. At this low solution concentration, the surface coverage of **DBA-OC26** is poor however the system still exists as densely packed network. The surrounding rows with smaller periodicity correspond to the co-adsorbed octanoic acid. Imaging parameters: V_{bias} = -200 mV, I_{set} = 0.28 nA.

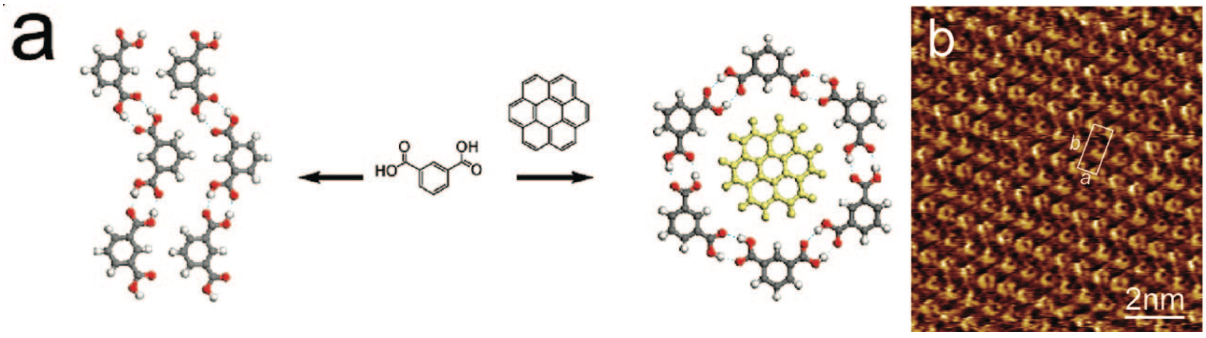

Figure S9: (a) Schematic showing the transition of the densely packed zigzag pattern of **ISA** in presence of **COR**. (b) STM image showing the dense zigzag pattern of **ISA** obtained in absence of **COR** at the octanoic acid/HOPG interface. Reproduced from Ref. 13 (*Nano Lett.* **2008,** *8,* 2541-2546).

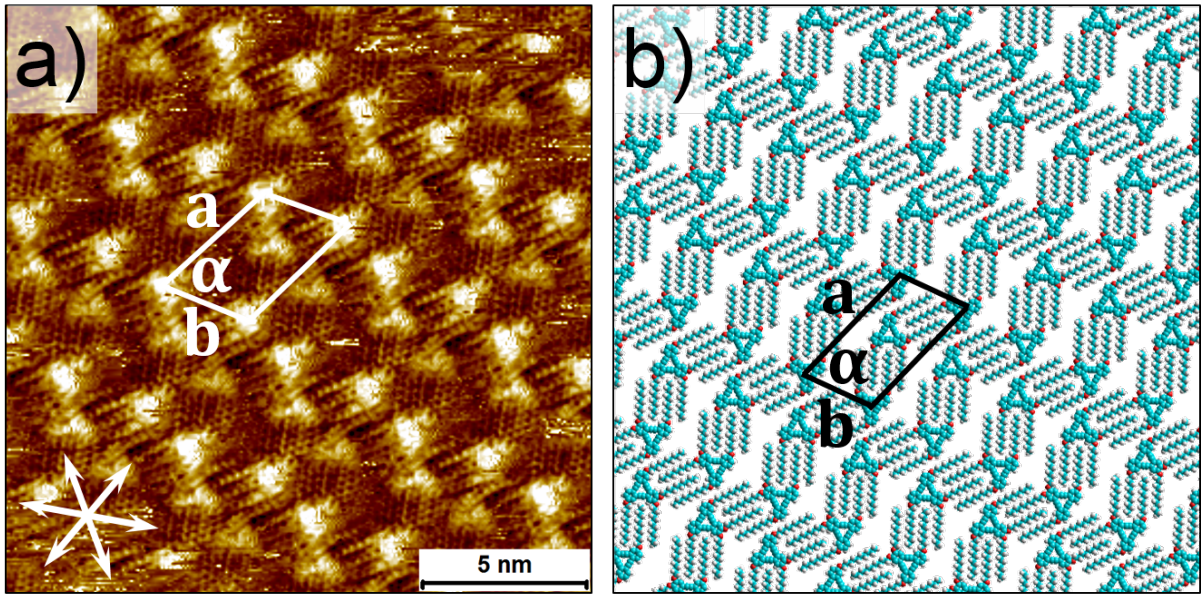

Figure S10: STM image of the densely packed network of **DBA-(4)-OC10** (3.0×10^{-6} M) obtained at the octanoic acid/HOPG interface in absence of **COR-ISA.** The graphite symmetry axes are shown in the lower left corner. The unit cell is overlaid on the STM image and the cell parameters are: a = 4.2±0.1 nm, b= 2.3±0.1 nm and α = 71±1.0°. Imaging parameters: V_{bias} = 300 mV, I_{set} = 0.28 nA. (b). Molecular model showing the arrangement of **DBA-(4)-OC10** molecules in the self-assembled monolayer.

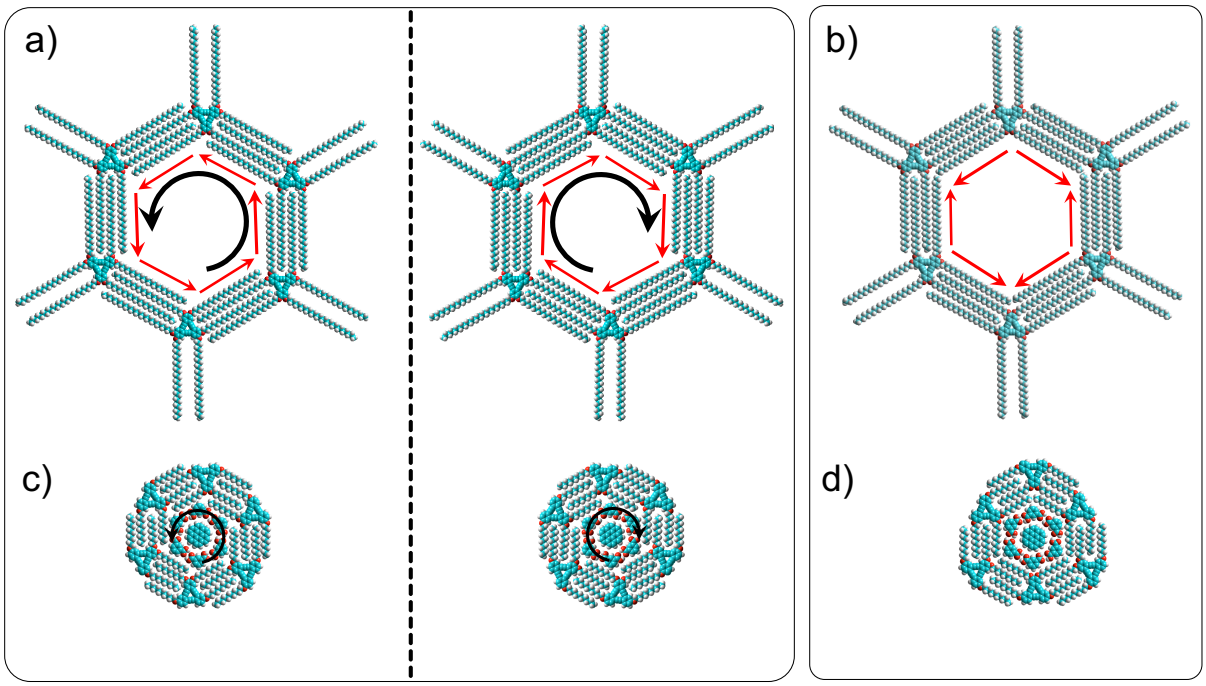

Figure S11: Chirality of DBA nanowells. (a). A virtual "clockwise" (CW) or "counterclockwise" (CCW) nanowell is obtained by combining two distinct interdigitation patterns. The labels CW and CCW refer to the sense of rotation of the six alkyl chains making up the inner rim of the nanowell, and typically, the chirality of the nanowells is domain specific. (b). An achiral nanowell. The predominant formation of such distorted nanowells was first reported by us in the case of **DBA-OC10-ISA-COR** self-assembled networks formed on Au(111) (*ACS Nano*, 2012, **6**, 8381-8389). We note that the distorted nanowells for **DBA-OC26** observed in the present case exhibit more random interdigitation pattern as evident from Figure S12. (c). Chirality of the **DBA-(4)-OC10-ISA-COR** system. (d) Molecular model for the distorted achiral three component cluster.

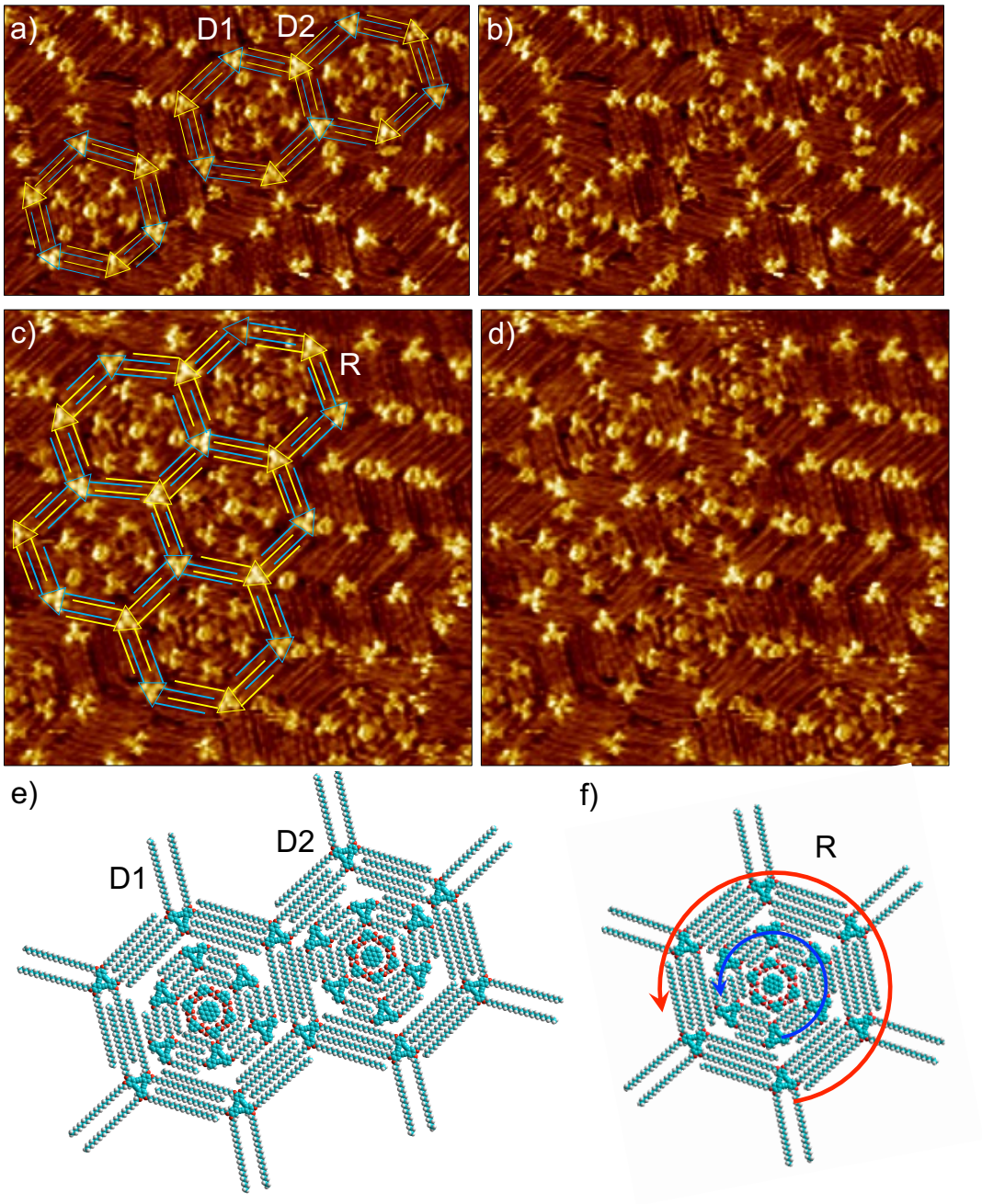

Figure S12: STM images showing the transfer of structural information between the inner to the outer shells. Note that when the inner shell of **DBA-(4)-OC10** is ordered (regular, **R**), the handedness of the outer shell often matches with that of the inner shell (also see STM image provided in the main text, Figure 4). However, there are rare exceptions. See for example, the lowest marked hexagon in (c), where the chirality of the inner and outer DBA shell is opposite. When the inner shell is distorted (**D1**, **D2**), the outer shell shows distortion as well. (a) STM image with markers highlighting the interdigitation pattern (b) Same STM image as in (a) without markers (c) STM image with markers highlighting the interdigitation pattern (d) Same STM image as in (c) without markers. (e) and (f) Molecular models that reproduce the disordered **(D1, D2)** and regular chiral **(R)** hexagons.

^{1}H and ^{13}C NMR Spectra of New Compounds.

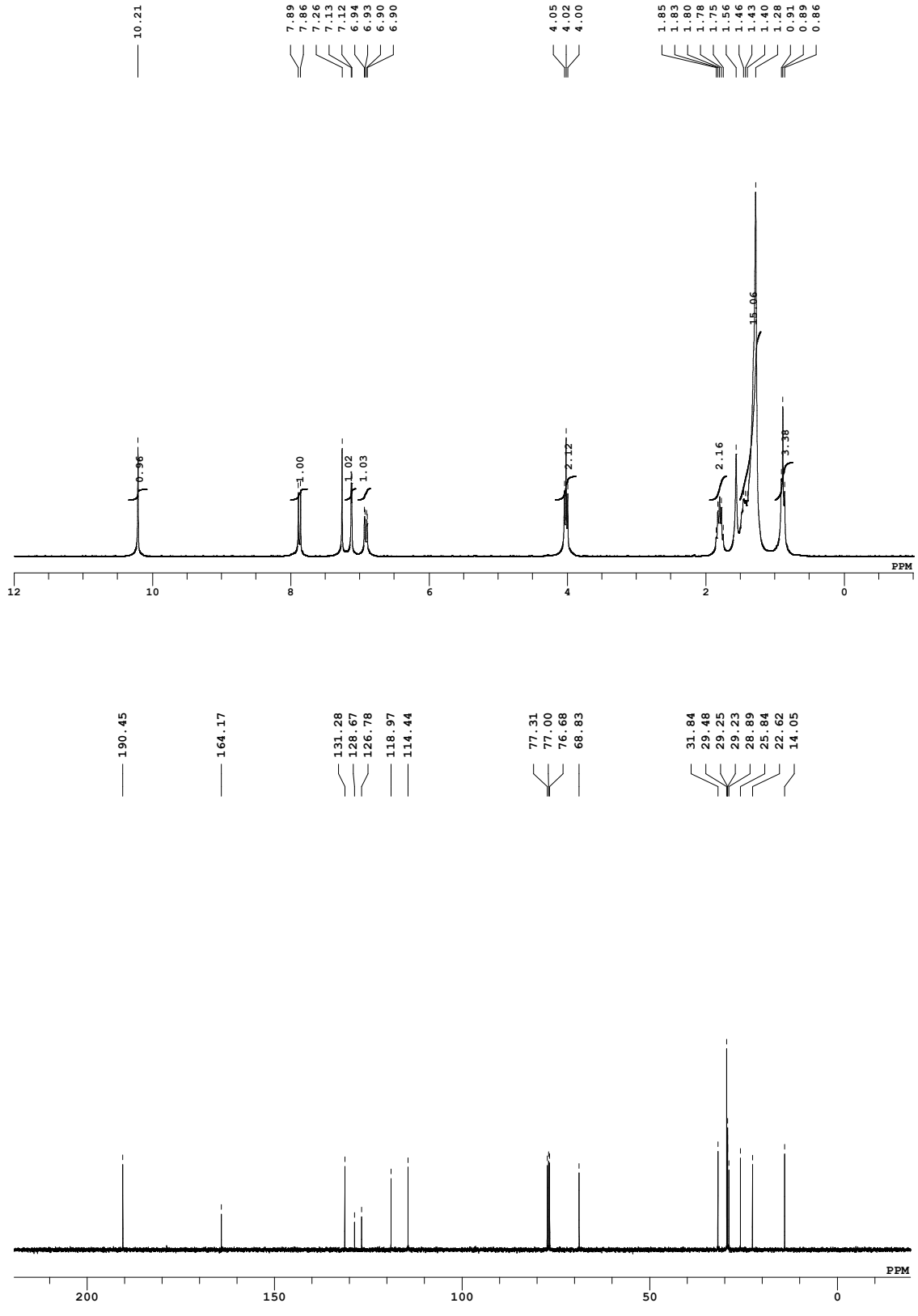

Figure S13. ^{1}H and ^{13}C NMR spectra of 2-bromo-4-decyloxybenzaldehyde in $CDCl_3$ at 30 °C.

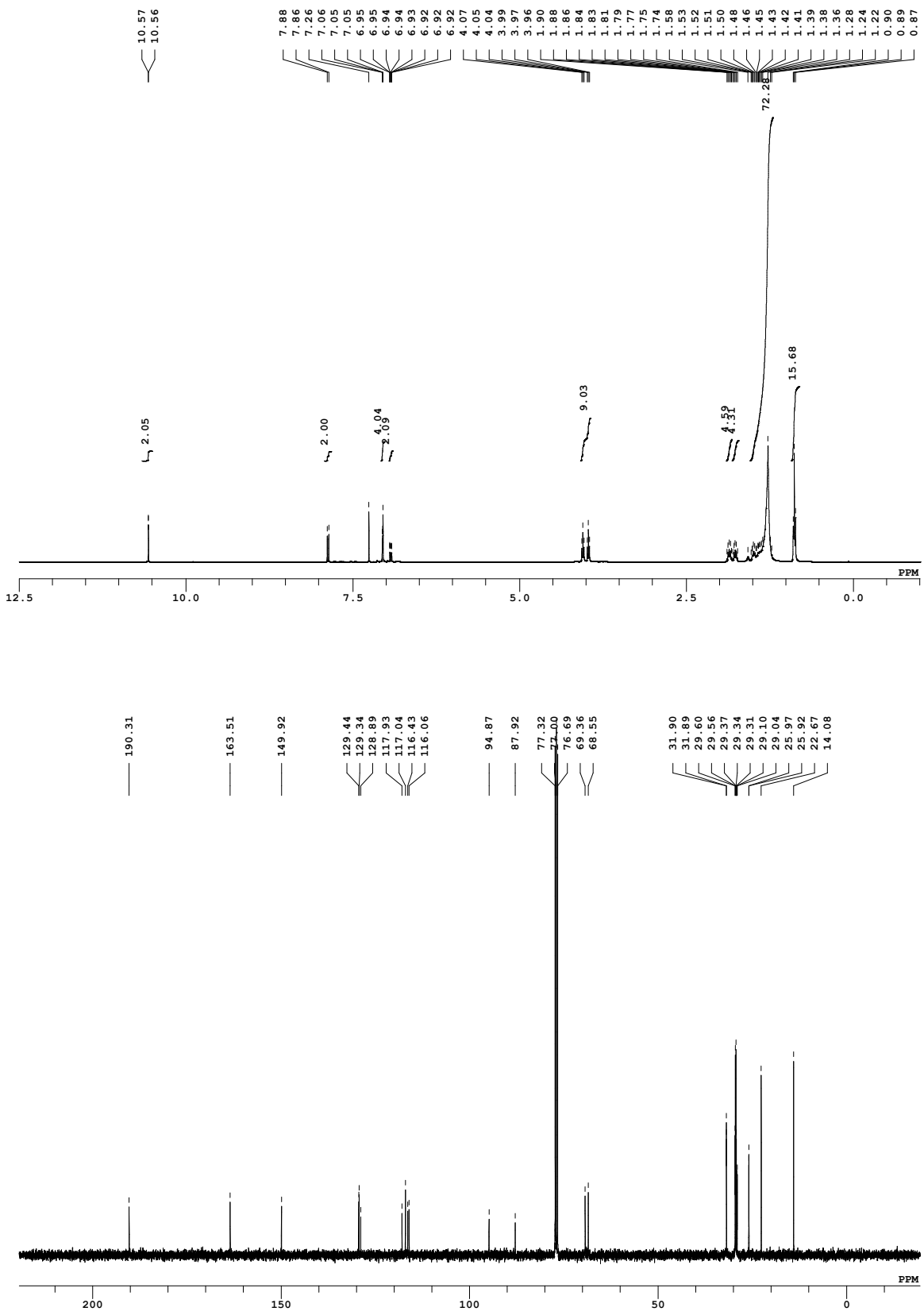

Figure S14. ^{1}H and ^{13}C NMR spectra of **S1** in $CDCl_3$ at 30 °C.

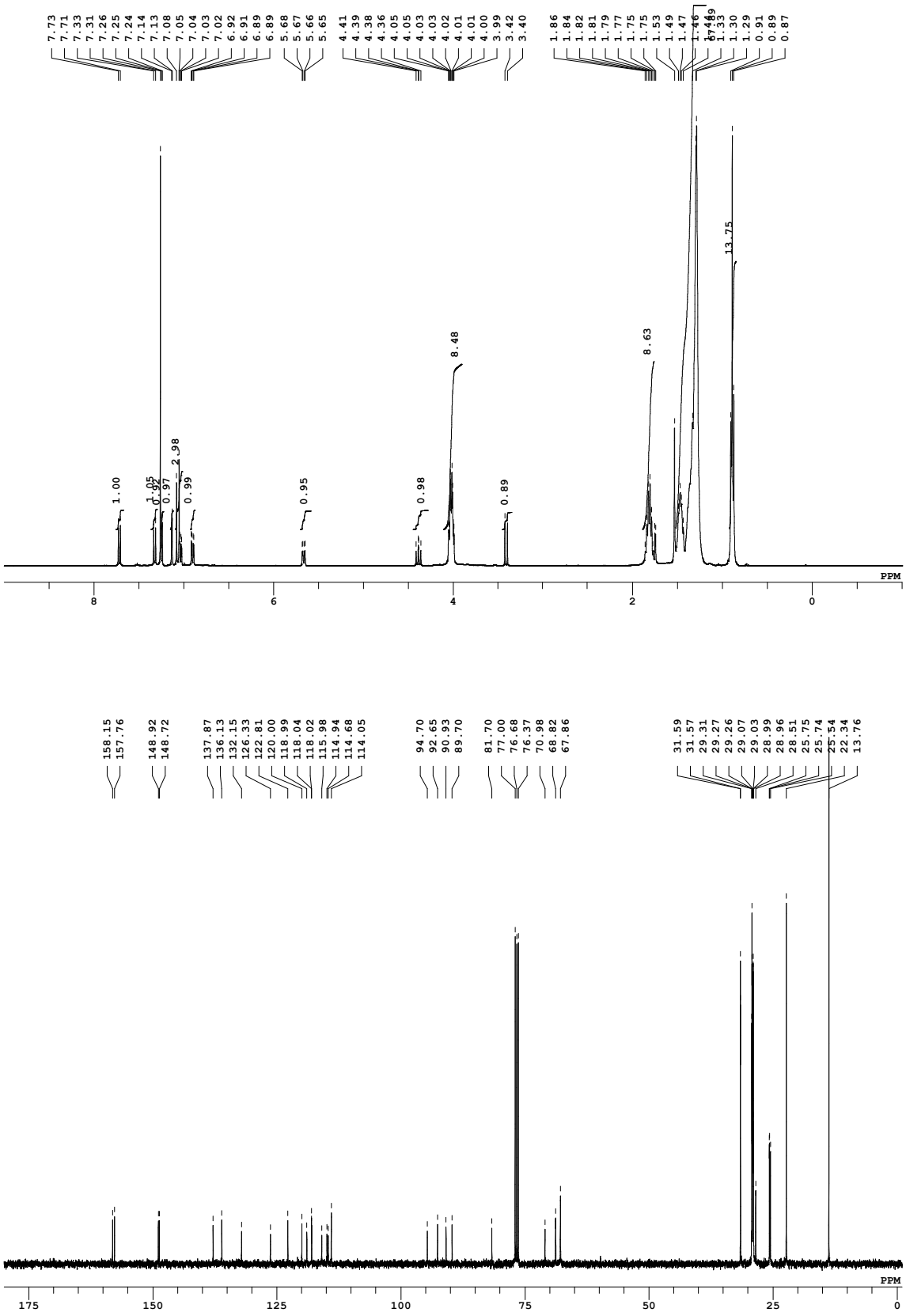

Figure S15. ^{1}H and ^{13}C NMR spectra of **S2** in $CDCl_3$ at 30 °C.

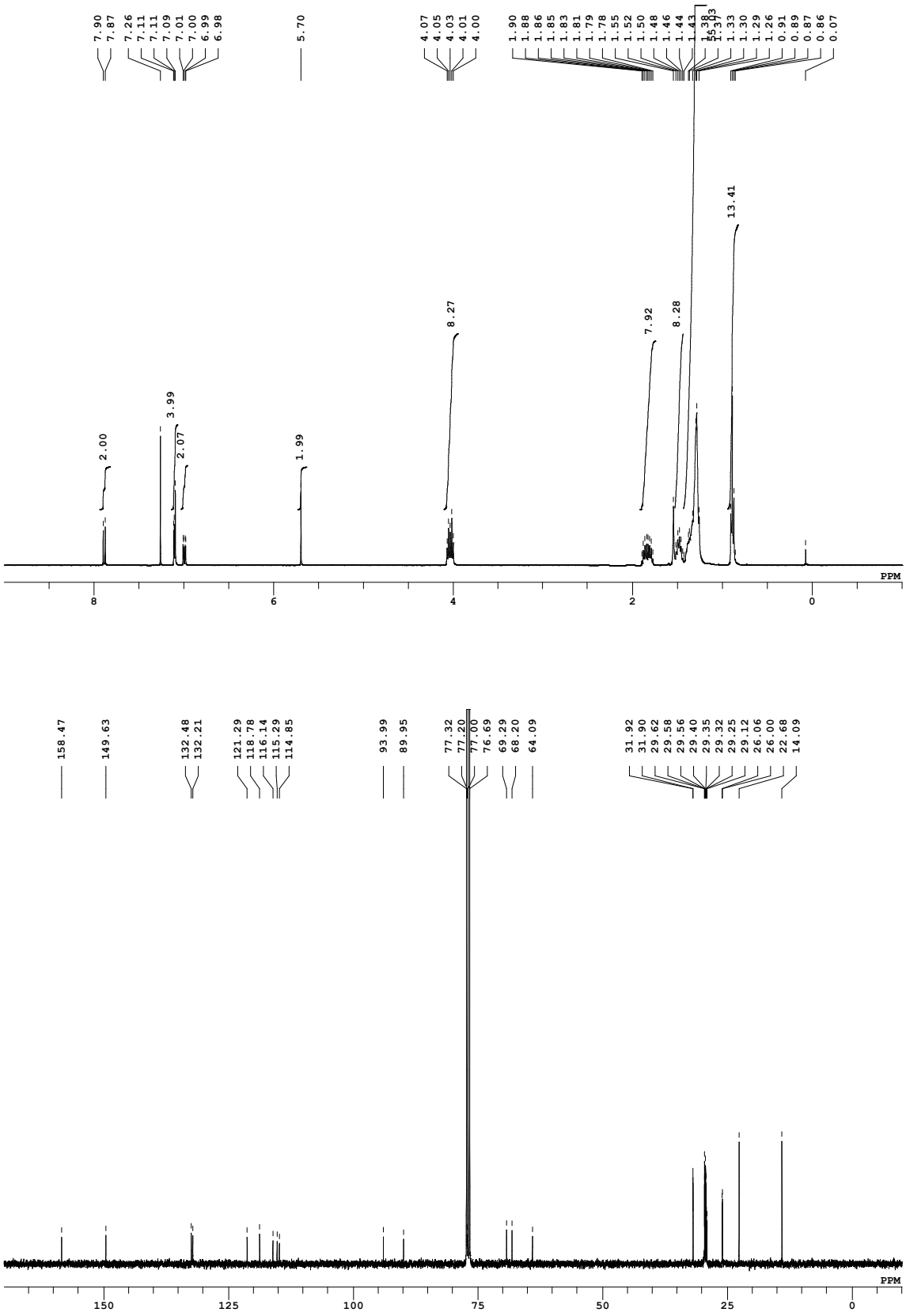

Figure S16. ^{1}H and ^{13}C NMR spectra of **S3** in $CDCl_3$ at 30 °C.

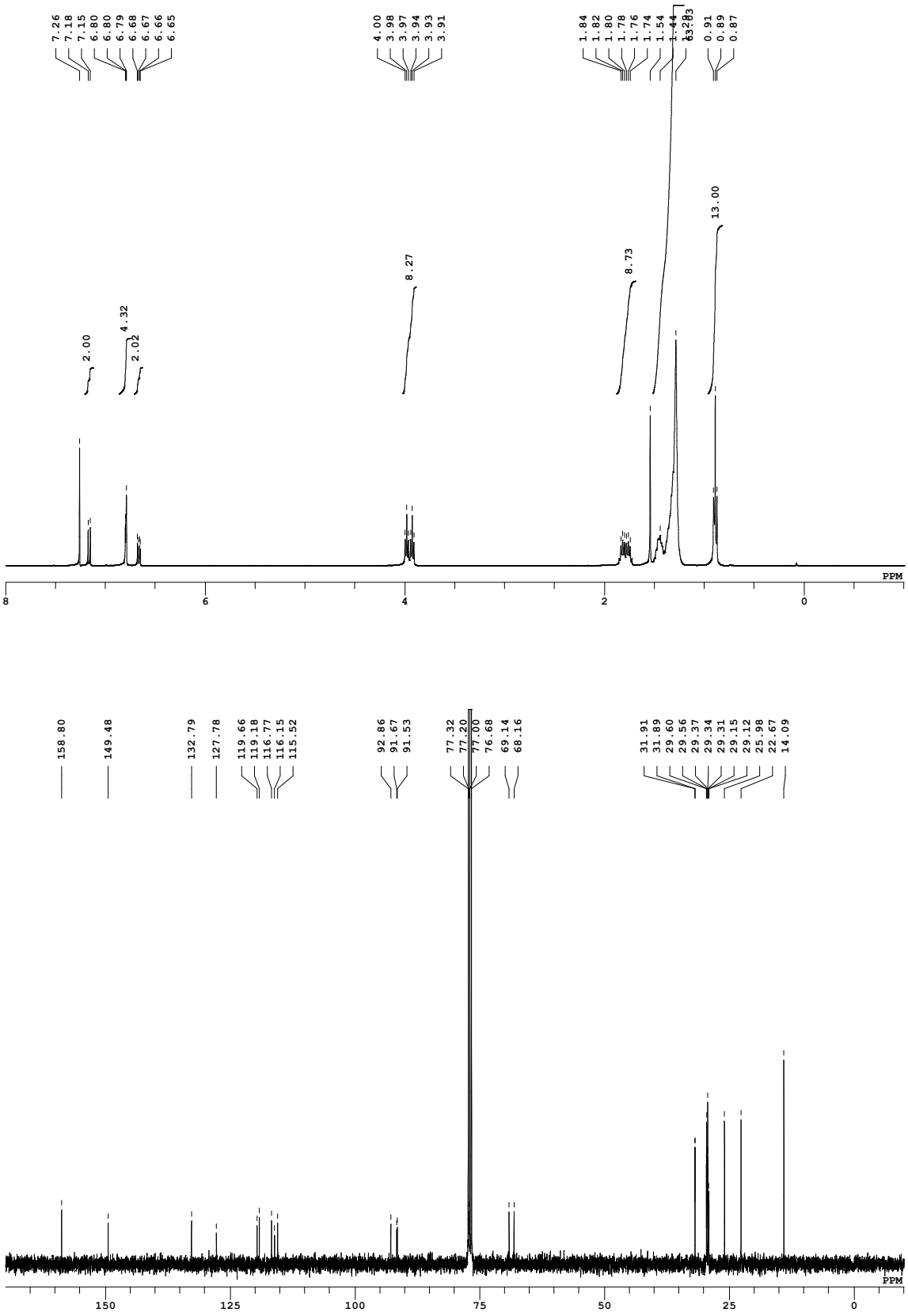

Figure S17. ^{1}H and ^{13}C NMR spectra of **DBA-(4)-OC10** in $CDCl_3$ at 30 °C.

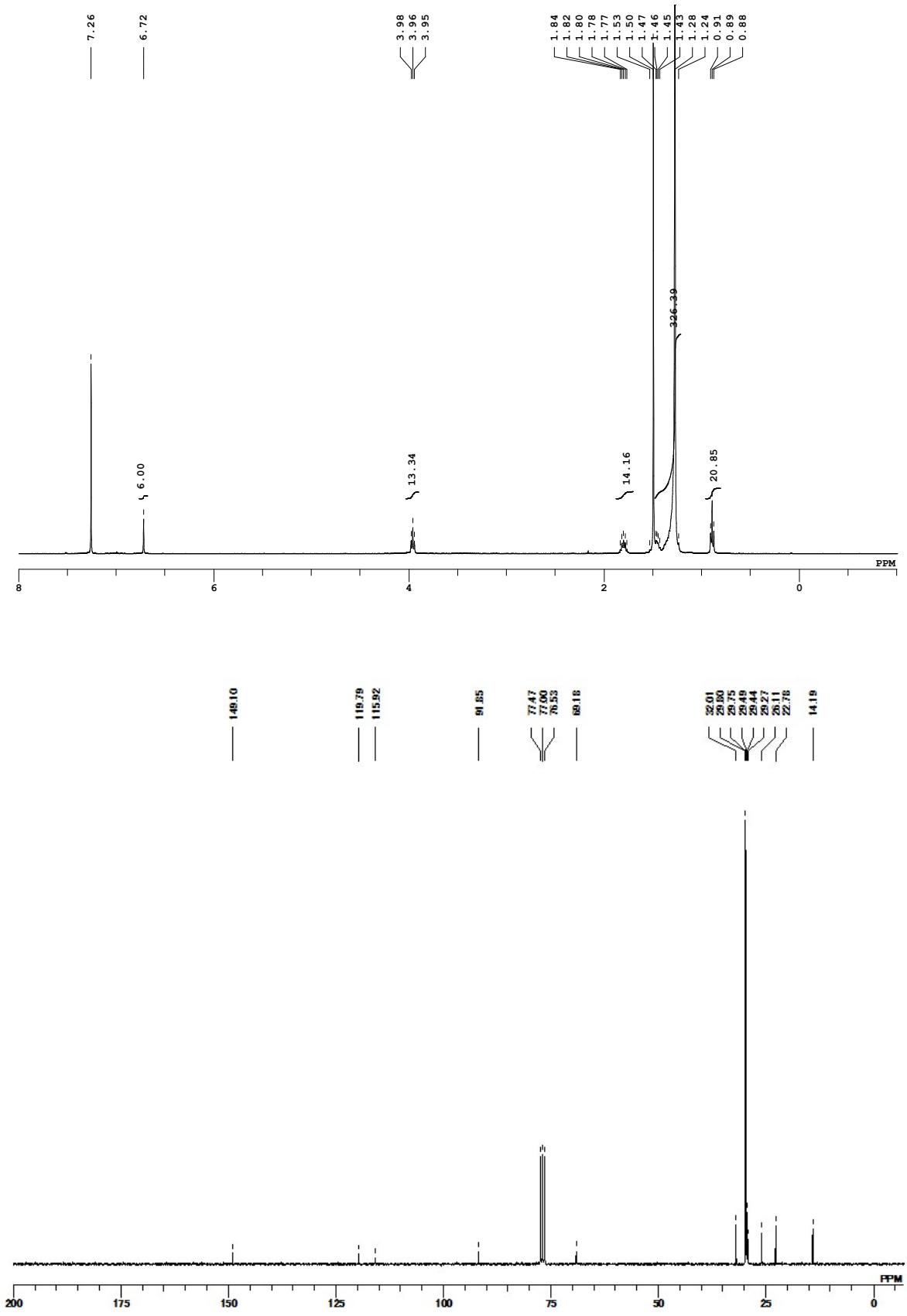

Figure S18. ^{1}H and ^{13}C NMR spectra of **DBA-OC26** in $CDCl_3$ at 50 °C.

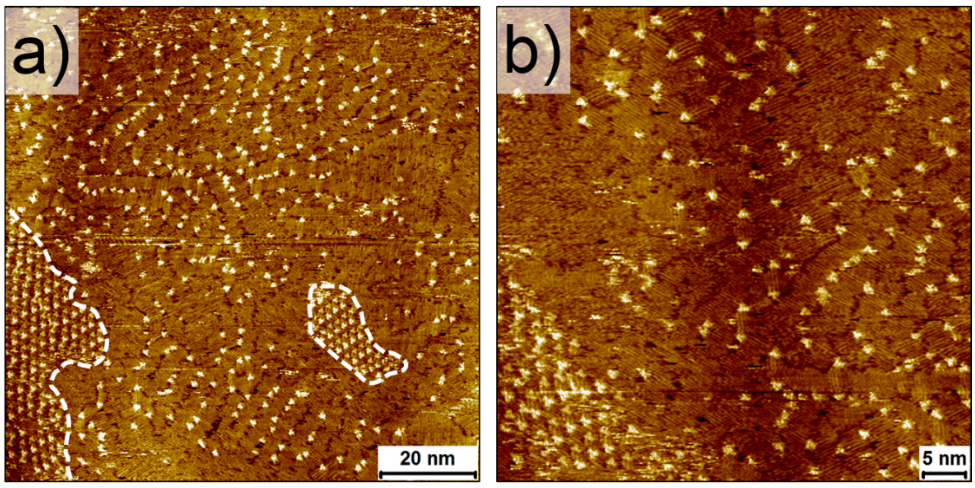

Fig. S19 Representative large and small-scale STM images of the **DBA-OC26-DBA-(4)-OC10-ISA** system obtained at the octanoic acid/HOPG interface. Solution composition: **DBA-OC26** (2.8×10^{-6} M), **DBA-(4)-OC10** (3.2×10^{-6} M) and **ISA** (2.7×10^{-4} M). Imaging parameters: V_{bias} = 300 mV, I_{set} = 0.28 nA. It is clearly evident that preferential adsorption of **DBA-OC26** and **DBA-(4)-OC10** occurs and **ISA** is not adsorbed at all. Phase separated domains of **DBA-OC26** and **DBA-(4)-OC10** are formed. White dotted lines separate the densely packed network of **DBA-(4)-OC10** from the densely packed network of **DBA-OC26**.

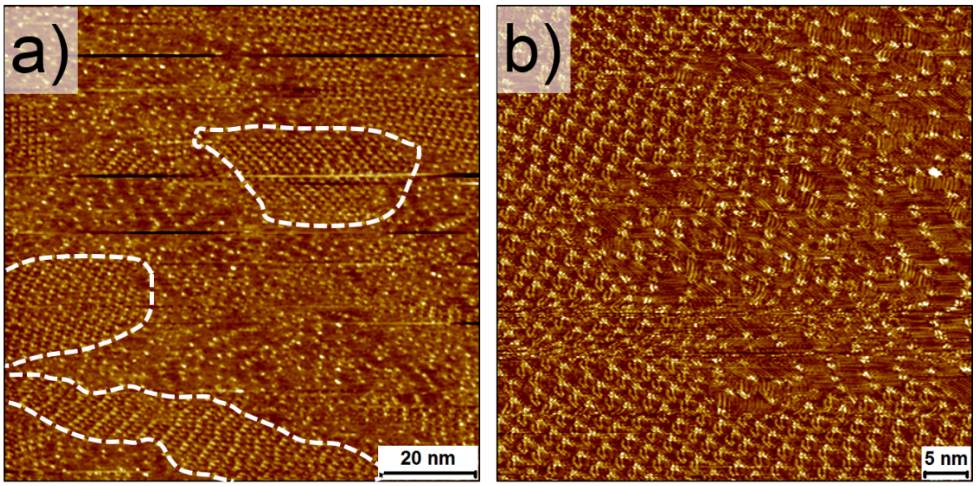

Fig. S20 Representative large and small-scale STM images of the **DBA-OC26-DBA-(4)-OC10** system obtained at the octanoic acid/HOPG interface. Solution composition: **DBA-OC26** (2.8×10^{-6} M) and **DBA-(4)-OC10** (3.2×10^{-6} M). Imaging parameters: V_{bias} = 400 mV, I_{set} = 0.27 nA. It is clearly evident that presence of **DBA-(4)-OC10** in the solution mixture does not induce porous network formation in the case of **DBA-OC26** on the surface in absence of **ISA-COR** guest cluster. Phase separated domains of **DBA-OC26** and **DBA-(4)-OC10** are formed. White dotted lines separate the densely packed network of **DBA-(4)-OC10** from the densely packed network of **DBA-OC26**.

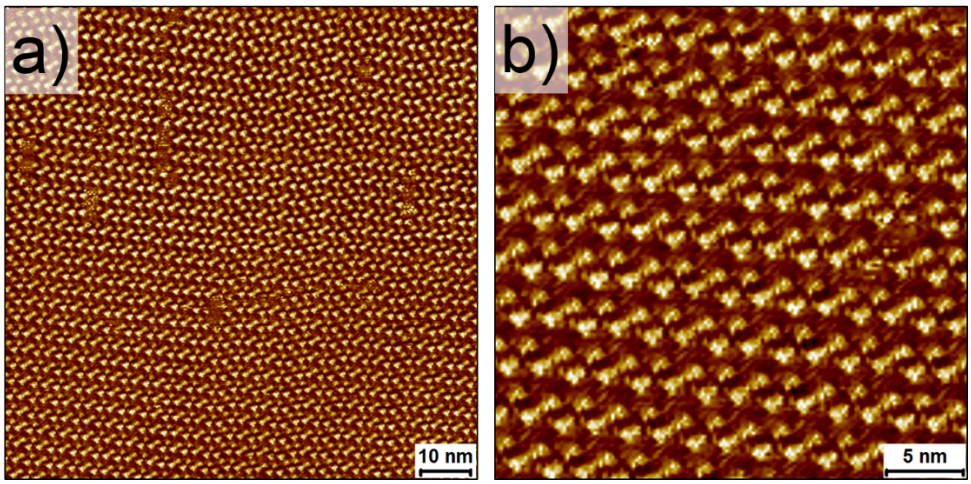

Fig. S21 Representative large and small-scale STM images of the **DBA-(4)-OC10-ISA** system obtained at the octanoic acid/HOPG interface. Solution composition: **DBA-(4)-OC10** (3.2×10^{-6} M) and **ISA** (2.7×10^{-4} M). Imaging parameters: V_{bias} = 400 mV, I_{set} = 0.28 nA. It is clearly evident that the **ISA** alone does not induce the formation of porous **DBA-(4)-OC10** network on the surface without **COR** guest species. Preferential adsorption of densely packed network of **DBA-(4)-OC10** is observed.